Journal of Medicinal Chemistry

pubs.acs.org/jmc Article

Novel Targeted Photosensitizer as an Immunomodulator for Highly Efficient Therapy of T-Cell Acute Lymphoblastic Leukemia

Gankun Yuan, Mengyu Yao, Huihui Lv, Xiao Jia, Juanjuan Chen,* and Jinping Xue*

Cite This: https://dx.doi.org/10.1021/acs.jmedchem.0c01072 Read Online

ACCESS | Metrics & More | Article Recommendations | Supporting Information

ABSTRACT: Dasatinib is a kinase-targeted drug used in the treatment of leukemia. Regrettably, it remains far from optimal medicine due to insurmountable drug resistance and side effects. Photodynamic therapy (PDT) has proven that it can induce systemic immune responses. However, conventional photosensitizers as immunomodulators produce anticancer immunities, which are inadequate to eliminate residual cancer cells. Herein, a novel compound **4** was synthesized and investigated, which introduces dasatinib and zinc(II) phthalocyanine as the targeting and photodynamic moiety, respectively. Compound **4** exhibits a high affinity to CCRF-CEM cells/tumor tissues, which overexpress lymphocyte-specific protein tyrosine kinase (LCK), and preferential elimination from the body. Meanwhile, compound **4** shows excellent photocytotoxicity and tumor regression. Significantly, compound **4**-induced PDT can obviously enhance immune responses, resulting in the production of more immune cells. We believe that the proposed manner is a potential strategy for the treatment of T-cell acute lymphoblastic leukemia.

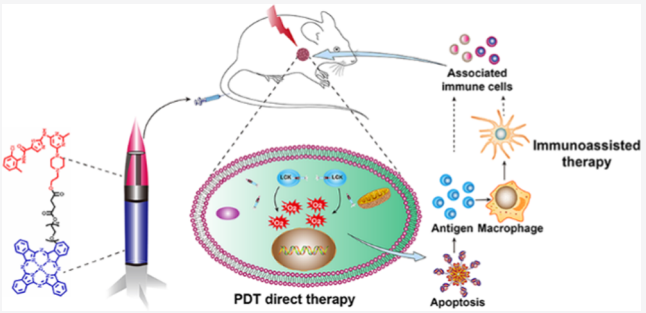

INTRODUCTION

Acute lymphoblastic leukemia (ALL) is a malignant tumor disease in which B-line or T-line cells derived from lymphocytes abnormally proliferate in the bone marrow.[1−3] Abnormally proliferating primitive cells can aggregate in the bone marrow, inhibit normal hematopoietic function, and spread to the whole body through the blood circulation. T-cell acute lymphoblastic leukemia (T-ALL) is a common type of ALL, which seriously endangers the physical and mental health of human beings.[4,5] Currently, chemotherapy, radiation therapy, and bone marrow transplantation are the main clinical treatment methods. Specifically, tyrosine kinase inhibitors are the most used and direct chemotherapeutic drugs.[6−9] Dasatinib, a second-generation small-molecule-targeted tyrosine kinase inhibitor, exhibits a wide range of targets, such as BCR-ABL kinase, SRC family kinases (SRC, LCK, YES, FYN), etc.[10−12] Lymphocyte-specific protein tyrosine kinase (LCK), a member of SRC family kinases, shows abnormally high expression in T-ALL cells, surpassing that in other leukemia or normal T cells. It has been reported that dasatinib can accurately target and reduce the activity of LCK kinase, which results in cell proliferation inhibition.[13−18] However, it is still far from an optimal drug due to insurmountable drug resistance and significant side effects (such as nausea, vomiting, diarrhea, rashes, and liver toxicity) after long-term usage.[19−21] Therefore, it is urgent to develop a new and effective strategy for the treatment of T-ALL.

Photodynamic therapy (PDT) is an emerging and promising treatment option for cancers and some noncancerous diseases. It utilizes photosensitizers (PSs) and the special wavelength of light and oxygen to generate reactive oxygen species (ROS) to ablate cancer cells.[22−25] In comparison with traditional treatment methods, PDT exhibits some unique and desirable properties, such as fewer side effects, no drug resistance, and minimal trauma.[26,27] Over the past few decades, it has been reported that PDT can promote anticancer immune responses through cancer-associated antigens produced from cancer cell residues.[28−34] In particular, under the stimulation of PDT, activated dendritic cells (DCs) can induce acute inflammation and migrate to lymph nodes, which can activate T cells and B cells and cause adaptive immune responses.[35−38] Thus, during the PDT process, the photosensitizers can be regarded as immunomodulators due to their effect on the immune responses.[39] However, the degree of immune responses produced by conventional photosensitizers is usually insufficient and needs to be further improved to eradicate residual tumor cells.[38] In addition, most photosensitizers used in PDT still face many challenges, such as poor tumor targeting, low singlet oxygen yield, and low efficacy in metastatic tumors,[40−43] hampering their application in clinical practice.

Received: July 6, 2020

https://dx.doi.org/10.1021/acs.jmedchem.0c01072
J. Med. Chem. XXXX, XXX, XXX−XXX

Scheme 1. Synthesis of Compounds 1−4[a]

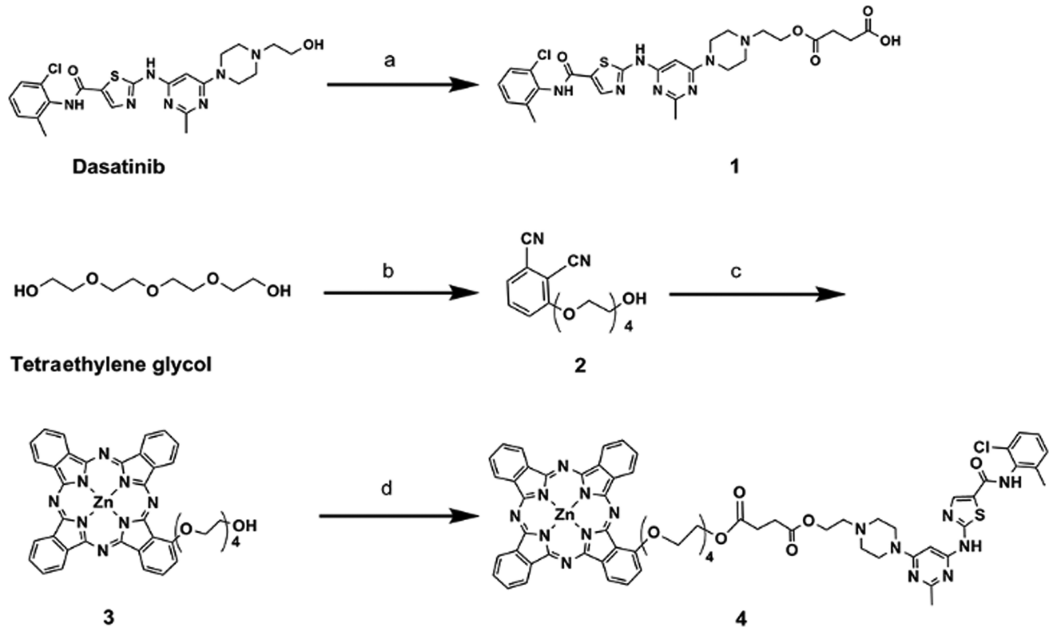

[a]Reagents and conditions: (a) dasatinib, succinic anhydride, triethylamine, DMF, room temperature (rt), 48 h, and 90%; (b) (i) K_2CO_3, 3-nitrophthalphthalonitrile, acetonitrile, and 70 °C and (ii) triethylene glycol, 90 °C, 7 h, and 65%; (c) phthalonitrile, n-pentanol, and 100 °C and (ii) $Zn(OAc)_2$, diazabicyclo[5.4.0]undec-7-ene, 130 °C, 7 h, and 12%; (d) **1**, EDCI, DMAP, DMF, rt, 24 h, and 7%.

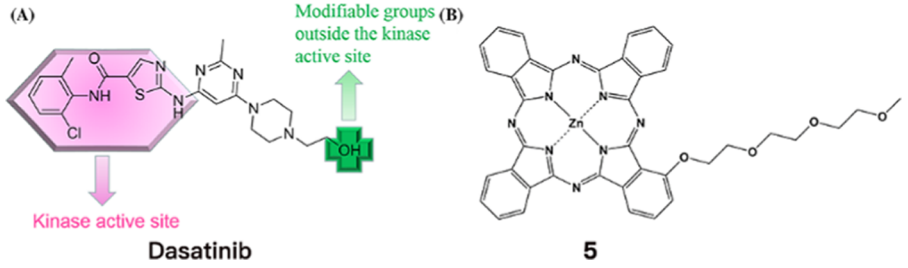

Figure 1. (A) Binding site of dasatinib to kinases (pink) and the modifiable functional group (green). (B) Chemical structure of the reference compound **5**.

Meanwhile, the photosensitizers have a long retention time in the body, which causes significant skin photosensitivity and damage to normal tissues.[44−46] Recently, photosensitizers have been demonstrated to be able to improve cancer targeting in PDT by combining biotargeting macromolecules[47−51] and nanomaterials.[52−56] However, their biological activity optimization and efficiency of biomolecules were limited due to their complex structure, variable inactivation, complex aggregation state, etc.[57] Additionally, the obstacles to their development for clinical trials are the toxicity of nanomaterials toward normal tissues/organs[58−61] and the metabolic block of some large-sized nanoparticles in the body.[62] Thus, it is necessary to formulate a novel photosensitizer with cancer-specificity, nontoxicity, high singlet oxygen generation, and easy elimination as an effective immunomodulator.

In recent years, some trials of PDT have been applied in the treatment of leukemia.[63−65] However, the strategy of small-molecule-targeted drug-mediated PDT for T-ALL has not been reported to the best of our knowledge. In this work, a novel anticancer conjugate that combined the efficient photosensitizer zinc(II) phthalocyanine with dasatinib was designed and synthesized to attack T-ALL. Dasatinib and zinc(II) phthalocyanine were used as the targeting and photodynamic moiety, respectively. Compound **4** was obtained by covalent linkage of the tetraethylene glycol chain. Then, its photophysical and photochemical properties and *in vitro* and *in vivo* tumor targeting and anticancer efficacy were investigated. Furthermore, the anticancer immune responses induced by **4** were examined by immunofluorescent staining. All results showed that **4** exhibits high singlet oxygen generation and cancer targeting, a remarkable anticancer effect, and strong immune responses. Moreover, preferential elimination from the body and negligible systemic toxicity of **4** were also found. Overall, our study provides a promising strategy to achieve targeting and highly efficient therapy of T-ALL.

RESULTS AND DISCUSSION

Synthesis. The synthetic route of compound **4** is shown in Scheme 1. Briefly, based on the functional and modifiable regions of dasatinib (Figure 1A),[66] zinc(II) phthalocyanine was attached to its hydroxyl group by the tetraethylene glycol chain to maintain the targeting ability of dasatinib and improve biocompatibility. First, compound **1** was obtained by ring-opening succinic anhydride and esterifying dasatinib under alkaline conditions. Under the catalysis of K_2CO_3, one terminal hydroxyl group of triethylene glycol was electrophilically

https://dx.doi.org/10.1021/acs.jmedchem.0c01072
J. Med. Chem. XXXX, XXX, XXX−XXX

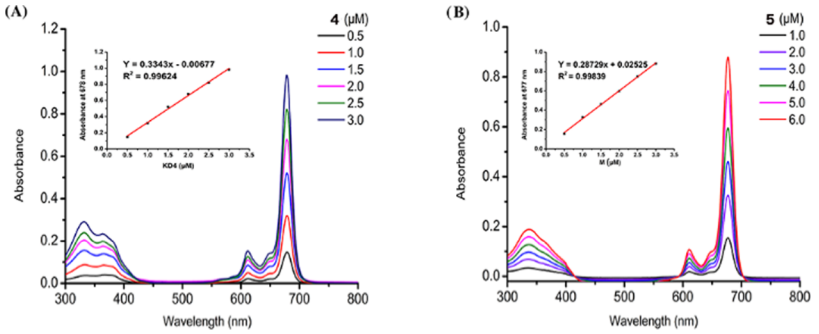

Figure 2. UV/vis absorption spectra of (A) **4** and (B) **5** at different concentrations in DMF. The inset shows the linear relationship of absorbance (Q band at 677 and 678 nm, respectively) and concentration (0.5−3.0 and 1.0−6.0 μM, respectively).

substituted with 3-nitrophthalonitrile to obtain compound **2**. Next, compound **2**, phthalonitrile, $Zn(OAc)_2$, and 1,8-diazabicyclo[5.4.0]undec-7-ene (DBU) were reacted in anhydrous n-pentanol. Finally, using compounds **3** and **1** as reactants, compound **4** was obtained by catalyzed esterification under 4-dimethylaminopyridine (DMAP) and 1-(3-dimethylaminopropyl)-3-ethylcarbodiimide hydrochloride (EDCI) in anhydrous *N*,*N*-dimethylformamide (DMF). The reference compound **5** (Figure 1B) was synthesized according to a previous report.[67] All new compounds were characterized by ^{1}H NMR, ^{13}C NMR, and high-resolution mass spectrometry (HRMS), and the purity of compounds **3**, **4**, and **5** was verified using high-performance liquid chromatography (HPLC).

Photophysical and Photochemical Characterization. Photophysical and photochemical properties of **4** and **5** were investigated. As shown in Figure 2, the Q bands in UV/vis absorption spectra of both compounds in DMF are sharp and intense with no observable new band (~710 nm for J-aggregation)[68−70] and exhibit typical electronic spectra of monomer zinc(II) phthalocyanine. Meanwhile, the absorption spectra of both compounds in phosphate-buffered saline (PBS) or Roswell Park Memorial Institute 1640 (RPMI-1640) medium are similar to those in DMF (Figures S1 and S2). Therefore, **4** and **5** are essentially free from aggregation not only in DMF but also in PBS and RPMI-1640 medium. Upon excitation at 610 nm, **4** and **5** showed a fluorescence emission band at 693 and 684 nm, respectively (Figure S3). All of the emission and absorption data are summarized in Table 1. The

Table 1. Photophysical/Photochemical Data of Compounds 4 and 5

compound	λ_{max}^{abs} (nm/log ε)	λ_{max}^{em} (nm)[a]	Φ_F[b]	Φ_Δ[c]
4	678/5.52	693	0.28	0.57
5	677/5.41	684	0.26	0.63

[a]Excited at 610 nm. [b]Using ZnPc as the standard in DMF (Φ_F = 0.28). [c]Using ZnPc as the standard in DMF (Φ_Δ = 0.56).[71]

fluorescence quantum yields (Φ_F) of **4** (0.28) and **5** (0.26) were approximately equal to that of standard unsubstituted zinc(II) phthalocyanine (0.28). Using 1,3-diphenylisobenzofuran (DPBF) as a capture agent for $^1O_2$, **4** and **5** have high singlet oxygen yields (0.57 and 0.63, respectively; Table 1 and Figure S4). These results showed that **4** still maintains the excellent photophysical and photochemical properties of zinc(II) phthalocyanine after introduction of the dasatinib moiety.

Cellular Uptake. To demonstrate the targeting ability of **4** at the cellular level, the CEM cells (human T-cell acute lymphoblastic leukemia cells CCRF-CEM; LCK is highly expressed) and HELF cells (human embryo lung fibroblast; LCK is lowly expressed) with different expression levels of LCK were selected. According to the dependence of uptake on time[72,73] and the data at different time points in Figure S5, 1 h was selected as a suitable time point for studying targeted uptake. First, the CEM cells were incubated with **4** and **5** (both at 1 μM) for 1 h, and then the intracellular fluorescence intensity of **4** and **5** under different conditions was measured by flow cytometry. As shown in Figure 3A, the fluorescence intensity of **4** was significantly higher (about five-fold) than that of **5**, which indicates the role of the dasatinib moiety in enhancing the cellular uptake of **4**. To further reveal whether the uptake of **4** in CEM cells is the LCK-mediated entry process, a competition test was conducted using dasatinib, which has an inhibitory effect on LCK and reduces the expression of LCK.[74,75] The CEM cells were pretreated with increasing concentrations of free dasatinib (0, 10, 20, 30, and 50 μM) for 1 h, followed by incubation with **4** (1 μM) for a further 1 h. As shown in Figure 3B, upon dasatinib pretreatment, the intracellular fluorescence intensity of **4** in CEM cells decreased with increasing concentrations of free dasatinib, implying that the uptake of **4** is suppressed. This result indicated that the LCK-mediated uptake pathway is the principal cellular entry pathway for **4**. Meanwhile, to reflect the selectivity of **4**, HELF cells were chosen as the control cell lines to co-incubate with CEM cells in the same cell dishes. Then, **4** and **5** (both at 1 μM) were added to the co-incubated cell culture dishes for 1 h. Their fluorescence intensity in CEM cells and HELF cells can be measured separately. As shown in Figure 3C, the fluorescence intensity of **4** in CEM cells was significantly higher (about five-fold) than that in HELF cells. In contrast, no significant difference in the fluorescence intensity of **5** was observed between the two kinds of cells (Figure 3D). These results indicated that the introduction of the dasatinib moiety can efficiently enhance the targeting and selection capabilities of zinc(II) phthalocyanine to T-ALL cells.

***In Vitro* Photodynamic Cytotoxic Activities.** To evaluate the *in vitro* photodynamic cytostatic activities, the Cell Counting Kit-8 (CCK-8) was used. Compounds **4** and **5** and dasatinib were incubated with CEM cells at the same concentration gradient (1−100 nM) for 1 h, separately. Then, the cells were irradiated under a light-emitting diode (LED) light source (λ = 670 nm, 4 mW·cm^{-2}, 0.48 J·cm^{-2}). The survival curves are shown in Figure 4A. It can be seen that **4** exhibits remarkable photocytotoxicity toward CEM cells than

https://dx.doi.org/10.1021/acs.jmedchem.0c01072
J. Med. Chem. XXXX, XXX, XXX−XXX

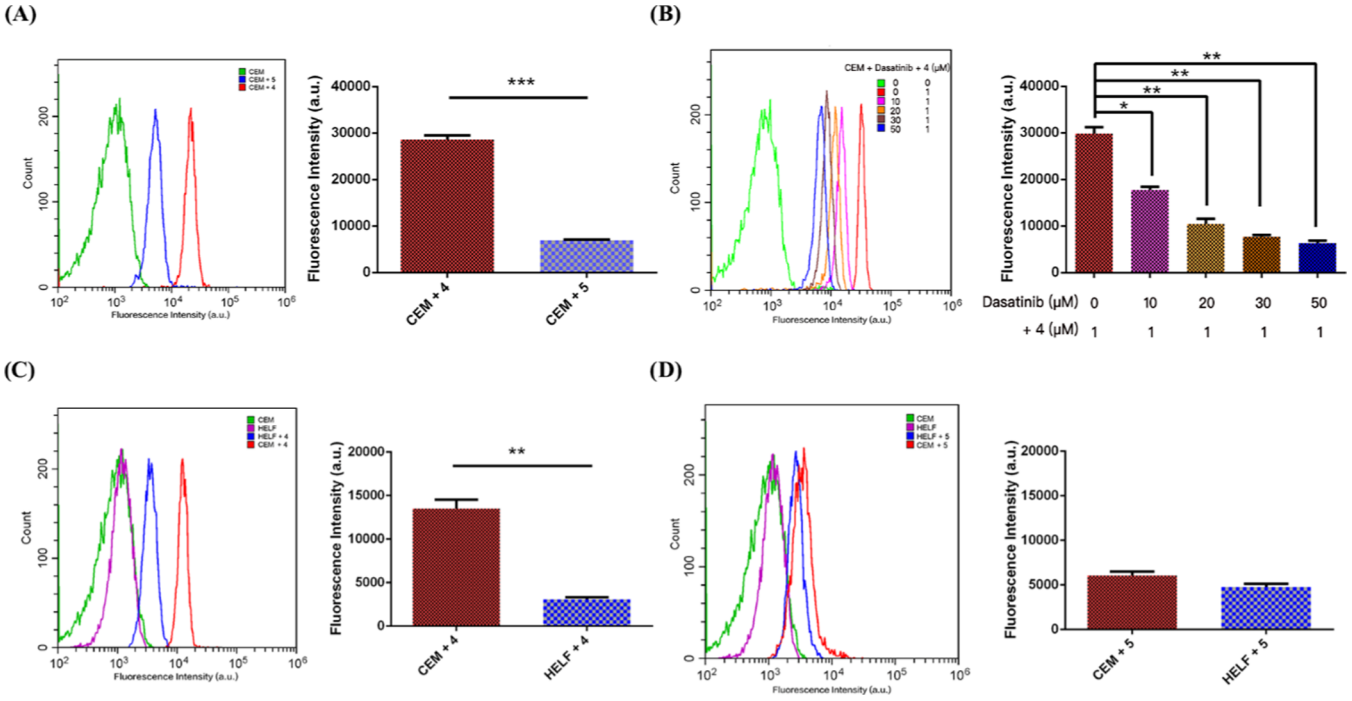

Figure 3. *In vitro* cellular uptake study. The fluorescence intensity profiles and the mean intracellular fluorescence intensities of (A) CEM cells incubated with **4** and **5** (both at 1 μM) for 1 h, (B) CEM cells pretreated with free dasatinib (0, 10, 20, 30, and 50 μM) for 1 h, followed by incubation with **4** (1 μM) for a further 1 h, (C) CEM and HELF cells co-incubated with **4** (1 μM) in the same cell culture dishes for 1 h, and (D) CEM and HELF cells co-incubated with **5** (1 μM) in the same cell culture dishes for 1 h. All of the experimental under the same conditions determined by flow cytometry. The compounds were in a culture medium with 0.78% *N*,*N*-dimethylacetamide (DMAC), 0.20% 1,2-propylene glycol, and 0.02% Cremophor EL (CEL) (v/v) prior to addition to the cells. Data are expressed as mean values ± standard error of mean (SEM) value of three independent experiments (*p < 0.05, **p < 0.01, ***p < 0.001).

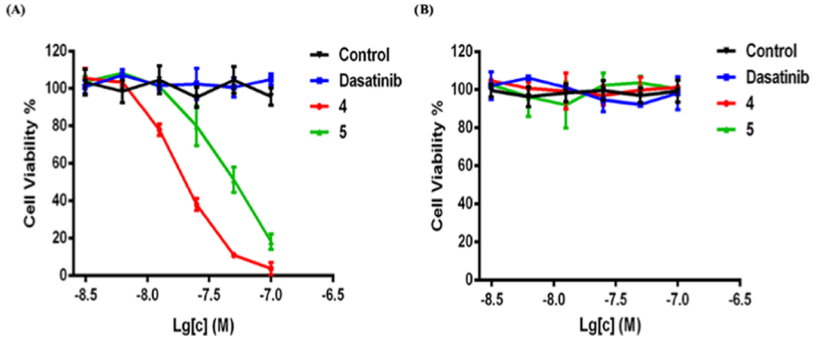

Figure 4. *In vitro* photodynamic activities. (A) Cytotoxicity toward CEM cells by incubation with **4**, **5**, dasatinib, and the control for 1 h under light illumination (λ = 670 nm, 4 mW·cm^{-2}, 0.48 J·cm^{-2}). (B) Cytotoxicity toward CEM cells by incubation with **4**, **5**, dasatinib, and the control for 1 h in the absence of irradiation. The compounds were in a culture medium with 0.1% or less mixed organic solvents (78% DMAC, 20% 1,2-propylene glycol, and 2% Cremophor EL) (v/v) prior to addition to the cells. Data are expressed as mean values ± standard error of mean (SEM) value of three independent experiments.

5, which may be caused by the higher uptake of **4**. The IC_{50} values of **4** and **5** (21.38 ± 0.83 and 63.04 ± 0.78 nM, respectively) are listed in Table 2. However, dasatinib did not exhibit cytotoxicity at the same concentration gradient (1−100 nM), and a much higher concentration (≥50 μM) was required for cytotoxicity to occur (Table 2 and Figure S6). At the same time, dark cytotoxicity experiments were performed under the same incubation conditions. The essential cytotoxicity of all compounds was not observed in the absence of irradiation (Figure 4B). Meanwhile, the photodynamic activities of all compounds toward HELF cells were also investigated. It was found that the photocytotoxicities of **4** and **5** toward HELF cells are low under light illumination (Figure S7), which was consistent with their low uptake in HELF cells. These results proved that **4** exhibits remarkable photocytotoxicity toward CEM cells and maintains the low dark cytotoxicity of zinc(II) phthalocyanine.

Table 2. IC_{50} Values for Compounds 4 and 5 and Dasatinib against CEM Cells

compound	4	5	dasatinib
IC_{50} (nM)[a]	21.38 ± 0.84	63.04 ± 0.81	335100.00 ± 0.76

[a]Under light illumination (λ = 670 nm, 4 mW·cm^{-2}, 0.48 J·cm^{-2}). Data are expressed as mean values ± standard error of mean (SEM) value of three independent experiments.

https://dx.doi.org/10.1021/acs.jmedchem.0c01072
J. Med. Chem. XXXX, XXX, XXX−XXX

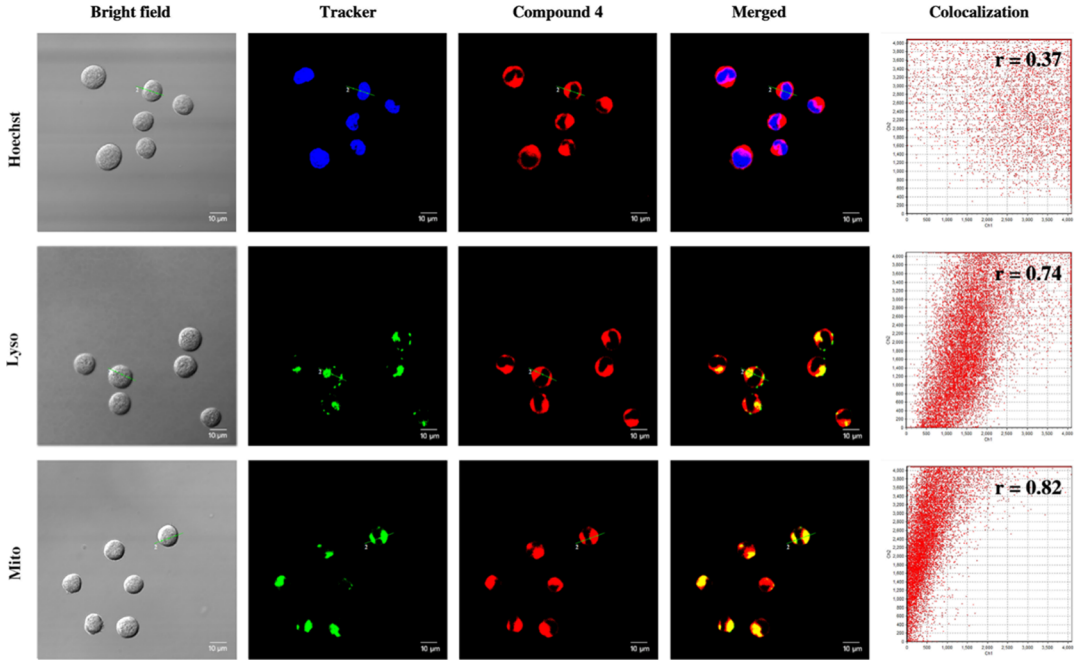

Figure 5. Confocal fluorescence images of CEM cells treated with Hoechst 33258, Lyso-Tracker DND-26, and Mito-Tracker Green FM (column 2) and **4** (column 3); the merged images (column 4) and the fluorescence colocalization of **4** with trackers traced along the green lines in the merged images (column 5, r = overlap ratio). The scale bar is 10 μm.

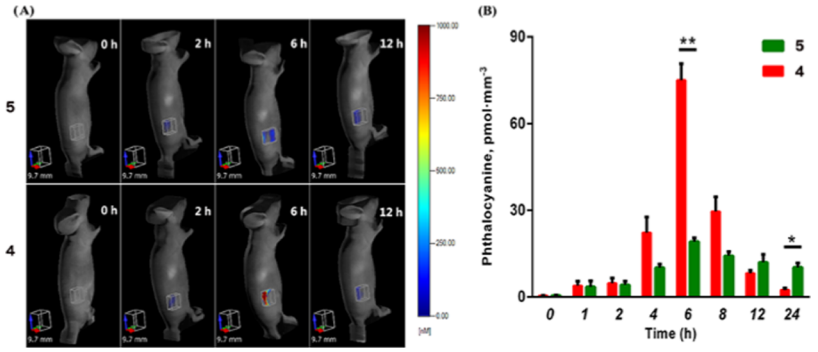

Figure 6. *In vivo* specificity study using nude mice bearing CEM tumors. (A) Three-dimensional fluorescence images based on FMT at 0, 2, 6, and 12 h after administration of **4** and **5**. (B) Changes in the mean tumor content of **4** and **5** over time were compared. Compounds **4** and **5** were present in PBS with 0.78% DMAC, 0.20% 1,2-propylene glycol, and 0.02% Cremophor EL (v/v) prior to injection in the mice. Data are presented as mean ± standard deviation (SD) (n = 3) ($^*p < 0.05$, $^{**}p < 0.01$, $^{***}p < 0.001$).

Subcellular Localization. ROS is the key and final agent to destruct tumor cells and tissues in the PDT process; however, it has a short lifetime and a limited diffusion radius.[76−80] Thus, the subcellular localization of photosensitizers is closely related to their cytotoxicity. Hoechst 33258 (excited at 405 nm, monitored at 425−475 nm), Lyso-Tracker DND-26, and Mito-Tracker Green FM (both excited at 488 nm, monitored at 510−570 nm) dyes were used as specific probes for the nucleus, lysosomes, and mitochondria, respectively, to study the intracellular distribution of **4** and **5** (both excited at 633 nm, monitored at 650−750 nm). As shown in Figure 5, the colocalization overlap of **4** with Lyso-Tracker DND-26 (0.74) or Mito-Tracker Green FM (0.82) was superior to that with Hoechst 33258 (0.37). These results demonstrated that **4** is mainly concentrated in the lysosomes and mitochondria but hardly found in the nucleus. Meanwhile, the intracellular distribution of **5** was observed to be almost similar to that of **4** (Figure S8).

***In Vivo* Tumor Tissue Targeting.** *In vivo* tumor-targeting ability of **4** was validated by *in vivo* fluorescence molecular tomography (FMT). Compound **4** and **5** were injected into nude mice bearing CCRF-CEM tumors via the tail vein. The fluorescence intensity of both compounds was detected (Figure 6A). As shown in Figure 6B, at 0−6 h post injection, both compounds showed an increasing trend of fluorescence intensity and reached their peak at 6 h. Compared to **5**, compound **4** exhibited a markedly faster increase rate. At 6 h, the tumor tissue content of **4** was approximately 75 pmol·mm^{-3}, which is about four-fold higher than that of **5** (19 pmol·mm^{-3}). Interestingly, at 6−8 h post injection, the content of **4** in the tumor tissues was quickly decreased to about 32 pmol·mm^{-3}, while **5** was only slightly reduced. At 8−24 h post injection, the fluorescence intensities of both compounds gradually decreased, and **4** was reduced at a faster speed. Additionally, at 24 h post injection, the residual fluorescence intensity of **4** was significantly lower than that of **5**. These

https://dx.doi.org/10.1021/acs.jmedchem.0c01072
J. Med. Chem. XXXX, XXX, XXX−XXX

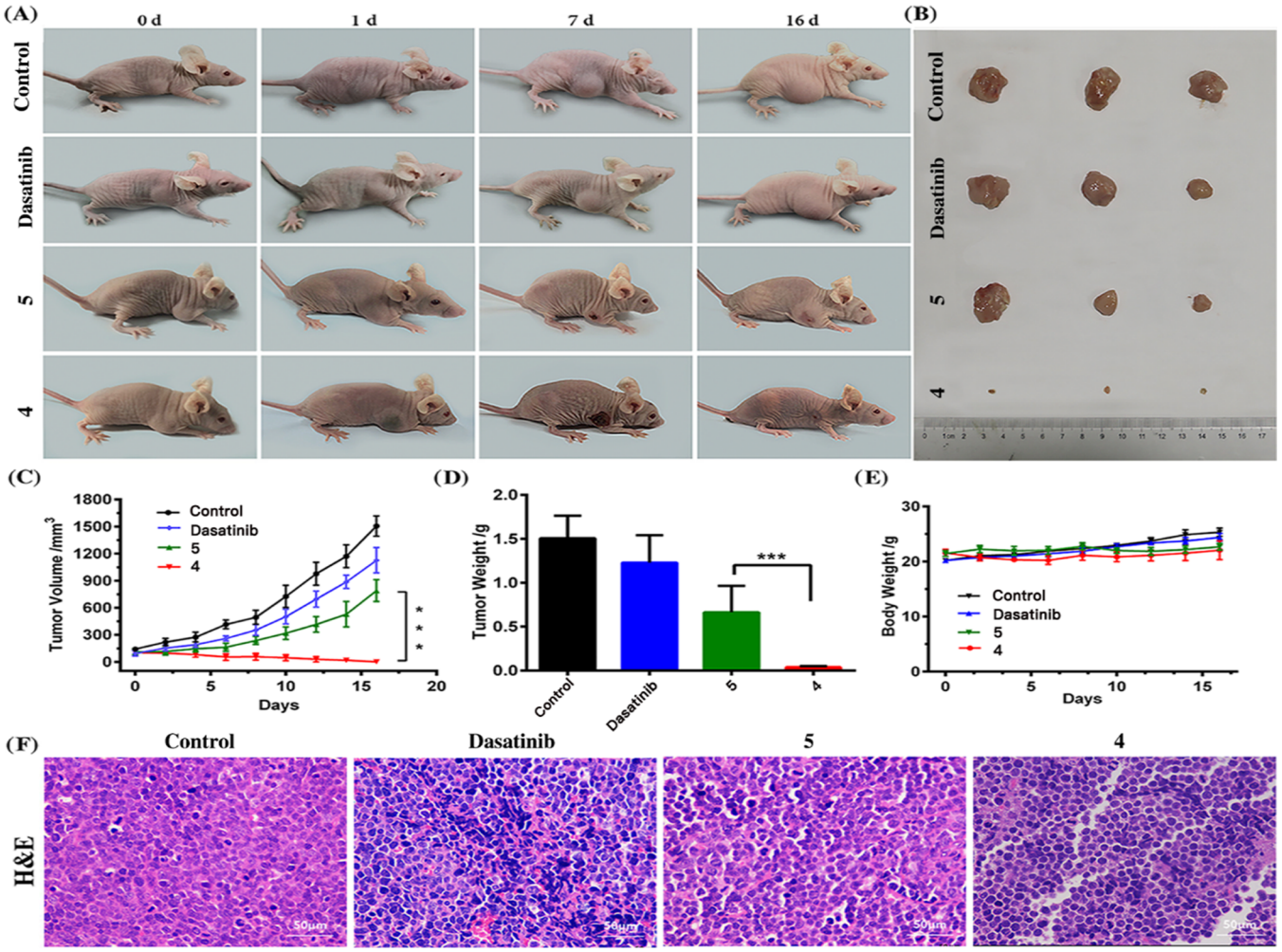

Figure 7. *In vivo* PDT study of nude mice bearing CEM tumors. (A) Photos of mice at 0, 1, 7, and 16 days post treatment. (B) Pictures of tumors stripped from mice at 16 days after treatment. (C) Tumor volume change curves after PDT treatment. (D) Average tumor weight after PDT treatment. (E) Body weight change curves of mice during 16 days. (F) Hematoxylin and eosin (H&E) staining of tumor tissues. The compounds were in PBS with 0.78% DMAC, 0.20% 1,2-propylene glycol, and 0.02% Cremophor EL (v/v) prior to injection in the mice. Data are presented as mean ± SD (n = 5) (*p < 0.05, **p < 0.01, ***p < 0.001). The scale bar is 50 μm.

results prove that **4** is superior to **5** in terms of tumor-targeting ability and elimination speed.

***In Vivo* Photodynamic Activities.** The anticancer efficacy of **4** was explored using nude mice bearing CCRF-CEM tumors. Mice were randomized into four groups: **4**, **5**, dasatinib, and the control. A 670 nm laser (50 mW·cm^{-2}, 10 min) was employed at 6 h post injection. The tumor sizes in the four groups were closely monitored every other day. As shown in Figure 7A,C, a gradual decrease of the tumor sizes in the **4** group was observed post treatment and the tumor almost completely disappeared after 16 days. However, for the **5** group, a certain tumor sluggish growth was displayed within the first 6 days post treatment but then accelerated after 6 days, which is due to an inhibitory effect induced by PDT in the early stage. The dasatinib group showed a feeble effect on tumor suppression, and the tumor size was slightly smaller than that of the control group, which is due to the low tumor suppression effect of dasatinib. Notably, in terms of the tumor size, the **4** group is remarkably smaller than that of the dasatinib group, which also indicates that **4** is superior to the chemotherapeutic drug alone under light illumination. Moreover, unlike multiple times of administration of chemotherapy, **4**-induced PDT only requires administration and irradiation once, and its anticancer effect can last for several days, which may be due to the continuous effect of ROS produced and the related immune response induced by PDT. The same results were confirmed by the stripped tumor volume and weight in the four groups after 16 days (Figure 7B,D). Meanwhile, histological analysis of tumor tissues in the four groups was conducted (Figure 7F). Evident necrosis was observed in the **4** group, which includes joint interspace widening, nuclei contraction, and the destruction of membrane integrity, indicating that the tumor tissues had been successfully destroyed. However, only a small extent of necrosis and vacuoles could be observed in **5** and dasatinib groups. All results suggested that the **4** group exhibits a significant anticancer effect than the other three groups.

To further verify the *in vivo* biosafety of **4**, the weight of the mice was measured during treatment. As shown in Figure 7E, a slight increase in weight in all groups was seen post treatment. Subsequently, the H&E staining results of other normal organ sections (Figure S9) showed that the **4** group has neither obvious signs of organ damage nor inflammation, which is the same as that of other groups. These results indicated that **4**

https://dx.doi.org/10.1021/acs.jmedchem.0c01072
J. Med. Chem. XXXX, XXX, XXX−XXX

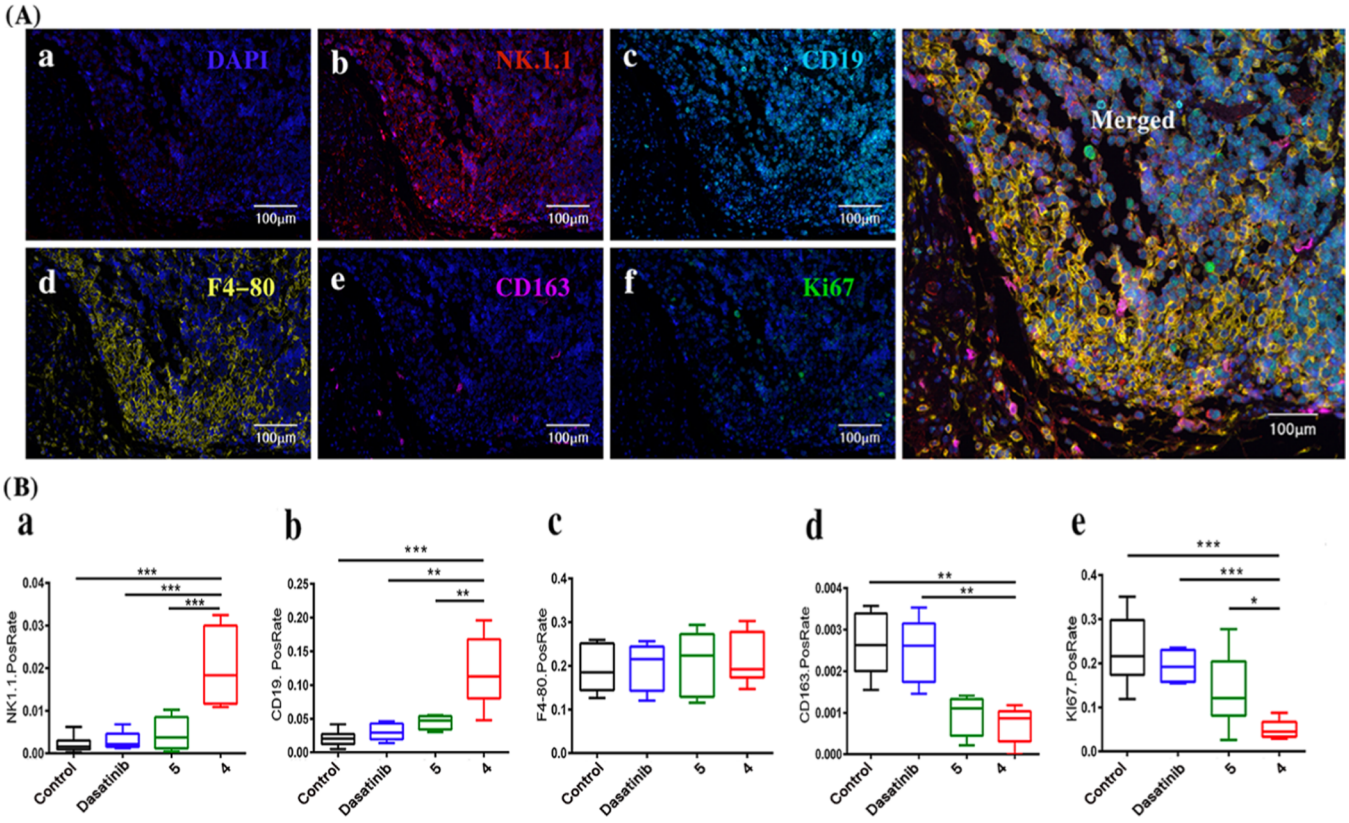

Figure 8. Immunohistochemical staining of tumor tissues sections. (A) Staining of different antibodies in the **4** group: (a) DAPI (blue), (b) NK1.1 (red), (c) CD19 (cyan), (d) F4−80 (yellow), (e) CD163 (pink), and (f) Ki67 (green). (B) Five antibodies' expression levels in the four groups: (a) NK1.1, (b) CD19, (c) F4−80, (d) CD163, and (e) Ki67. Data are presented as mean ± SD ($n = 3$) (*$p < 0.05$, **$p < 0.01$, ***$p < 0.001$). The scale bar is 100 μm.

shows no notable systemic toxicity *in vivo* with a high biosafety index.

Immunity Response Study. The anticancer immunity responses were further explored by immunohistochemical staining. The B cells are important immune cells in the immune system, whose main function is to mediate humoral immunity. In addition, it has been reported that natural killer (NK) cells and macrophages play key roles in immune responses.[81−84] NK cells are inherently capable of recognizing tumor cells without being contacted or activated in advance to exert their tumor-killing ability. Macrophages in different tissues are polarized to form different macrophage subtypes according to the environment, such as M1 macrophages and M2 macrophages. M1 macrophages can produce proinflammatory cytokine macrophages, which can promote immune function to inhibit tumor growth. In contrast, M2 macrophages are known as alternatively activated macrophages, which can inhibit immune function to promote angiogenesis and tumor growth.[85]

Therefore, 4′-6′-diamidino-2-phenylindole (DAPI) (for cell nucleus) and five different antibodies (NK1.1 for NK cells, CD19 for B cells, F4−80 for macrophages, CD163 for M2 macrophages, and Ki67 for tumor proliferation) were used to investigate the anticancer immunity responses of **4**. The images of immunohistochemical staining are shown in Figures 8A and S10−S12. The expression level of antibodies was quantified by their fluorescence intensity. First, for the expression level of NK1.1 and CD19 (Figure 8B-a,B-b), compared with the **5** group, the **4** group shows a significant increase. Meanwhile, the **5** group exhibits a slightly higher level compared to dasatinib and control groups, which confirms that no targeted photosensitizer-induced PDT can promote immune responses to a certain extent, but the effect is very faint. However, no obvious difference between the control and dasatinib groups were found. As shown in Figure 8B-c, the expression level of F4−80 antibody in all groups was basically the same, which indicates that the four groups have no significant effect on the expression of macrophages. Nevertheless, the expression levels of CD163 in **4** and **5** groups were obviously lower than those in the other two groups (Figure 8B-d), which implies that both the compounds induced less polarization to M2 macrophages. We speculated that PDT can inhibit the polarization to M2 macrophages to a certain extent, thereby indirectly inhibiting tumor growth. Furthermore, as shown in Figure 8B-e, the expression level of Ki67 in the **4** group was visibly lower than those in the other three groups, which further indicates that **4**-induced PDT results in stronger anticancer immune responses and significantly inhibits tumor proliferation. These results are also consistent with the *in vivo* photodynamic activity.

CONCLUSIONS

In summary, a novel anticancer target photosensitizer that combined zinc(II) phthalocyanine with the small-molecule-targeted drug dasatinib was designed and synthesized as an immunomodulator for the treatment of T-ALL. As expected, the results showed that **4** still maintained excellent photophysical and photochemical properties of ZnPc and the targeting ability of dasatinib. Due to the introduction of dasatinib, **4** can efficiently enhance the targeting and selection

https://dx.doi.org/10.1021/acs.jmedchem.0c01072
J. Med. Chem. XXXX, XXX, XXX−XXX

capabilities of zinc(II) phthalocyanine to T-ALL cells. The fast elimination rate of **4** from the body was demonstrated in nude mice bearing CCRF-CEM tumors. Meanwhile, compared with **5** and dasatinib, excellent photocytotoxicity in nanomolar concentrations and remarkable tumor regression of **4** were confirmed. Especially, **4** exhibited predominantly strong immune responses as an immunomodulator after administration, which may result in secondary destruction of cancer cells and produce systemic anticancer immunity. We believe that our study offers a promising therapeutic strategy for T-ALL. In the future, we will perform animal cardiopulmonary bypass model experiments for further research and promote the clinical application of **4**.

EXPERIMENTAL SECTION

General Methods. The reaction in the synthesis process was carried out under the protection of nitrogen. All solvents were of reagent grade and dehydrated using a purification system EX-SPS5−800 (EMINEX, Co., LTD). All new compounds were dissolved in DMSO-d_6 and tested for ^{1}H NMR and ^{13}C NMR spectra on an AVANCE III 400 MHz spectrometer. The chemical shift (δ) relative to TMS was expressed in parts per million (ppm). HRMS analysis was performed on an MSD X Series 2 ion trap mass spectrometer from Agilent Technologies Germany. The purity of compounds **3**, **4**, and **5** was measured using HPLC on an E2695 system (Waters). *In vitro* toxicity was tested using a Spectra Max i3x microplate reader. The UV/vis absorption spectra were obtained on a PerkinElmer UV spectrometer. Fluorescence spectra were measured using a Varian Kali Eclipse spectrometer. Intracellular localization was recorded on an Olympus FV1000 laser confocal microscope. Fluorescence imaging was obtained on a PerkinElmer fluorescence molecular tomography instrument (FMTTM 2500 LX).

*4-(2-(4-(6-((5-((2-Chloro-6-methylphenyl)carbamoyl)thiazol-2-yl)amino)-2-methylpyrimidin-4-yl)piperazin-1-yl)ethoxy)-4-oxobutanoic Acid (**1**).* Compound dasatinib (1.60 g, 3.27 mmol) and succinic anhydride (0.37 g, 3.70 mmol) were dissolved in 15 mL of DMF and stirred at room temperature (rt), and then triethylamine (0.70 g, 6.90 mmol) was added dropwise under nitrogen. The reaction was carried out for 48 h; the mixture was evaporated under vacuum, redissolved in CH_2Cl_2 (10 mL), and washed with CH_2Cl_2 (3 × 10 mL) and CH_3OH (3 × 40 mL). The product was evaporated to obtain a white solid compound **1** (1.73 g, 90%). ^{1}H NMR (400 MHz, DMSO-d_6): δ = 11.45 (s, 1H), 9.89 (s, 1H), 8.23 (s, 1H), 7.38 (d, J = 7.4 Hz, 1H), 7.27 (dd, J = 10.6, 7.5 Hz, 2H), 6.06 (s, 1H), 4.15 (t, J = 5.7 Hz, 2H), 3.50 (s, 4H), 2.58 (t, J = 5.7 Hz, 2H), 2.49 (s, 8H), 2.40 (s, 3H), 2.23 (s, 3H). ^{13}C NMR (101 MHz, DMSO-d_6): δ = 172.60, 165.63, 162.93, 160.41, 157.43, 141.34, 139.30, 134.03, 132.93, 129.48, 128.62, 127.47, 126.18, 83.12, 61.97, 58.95, 56.42, 53.18, 52.86, 44.04, 29.29, 26.05, 18.79. HRMS (ESI): m/z calculated for $C_{26}H_{30}ClN_7O_5S$ $[M + H]^+$, 588.1790; found, 588.1781.

*3-(2-(2-(2-(2-Hydroxyethoxy)ethoxy)ethoxy)-phthalonitrile (**2**).* Compound potassium carbonate (27.50 g, 200 mmol) and 3-nitrophthalphthalonitrile (8.70 g, 50 mmol) were dissolved in 15 mL of acetonitrile and heated to 70 °C. Triethylene glycol was then added and further heated to 90 °C for 7 h. The mixture was dried under reduced pressure, extracted with CH_2Cl_2 and brine, and purified using column chromatography (CH_2Cl_2/CH_3OH 30:1 v/v) to obtain a pale yellow solid compound **2** (10.45 g, 65%). ^{1}H NMR (400 MHz, DMSO-d_6): δ = 7.86 (t, J = 8.0 Hz, 1H), 7.68 (t, J = 7.9 Hz, 2H), 4.56 (s, 1H), 4.38 (s, 2H), 3.82 (s, 2H), 3.63 (s, 2H), 3.51 (q, J = 15.2, 7.7 Hz, 8H), 3.41 (s, 2H). ^{13}C NMR (101 MHz, DMSO-d_6): δ = 161.47, 136.22, 126.28, 119.33, 116.27, 115.86, 114.12, 103.46, 72.8, 70.58, 70.3, 70.28, 70.23, 69.94, 68.98, 60.69. HRMS (ESI): m/z calculated for $C_{16}H_{20}N_2O_5$ $[M + H]^+$, 321.1445; found, 321.1442.

*2-(2-(2-(2-(Zinc(II)phthalocyanine-1-yloxy)ethoxy)ethoxy)-ethoxy)ethan-1-ol (**3**).* Compound **2** (2.20 g, 6.80 mmol) and phthalonitrile (7.80 g, 61 mmol) were dissolved in 10 mL of anhydrous n-pentanol. The solution was stirred and heated to 100 °C until it became clear. Anhydrous $Zn(OAc)_2$ was then added, and the temperature was increased to 130 °C. Finally, 0.80 mL of DBU was added after the mixture turned green, and the reaction was continued for 7 h. The mixture was evaporated and purified using column chromatography (CH_2Cl_2/CH_3OH 20:1 v/v) to obtain a blue-black solid compound **3** (0.63 g, 12%). ^{1}H NMR (400 MHz, DMSO-d_6): δ = 9.25 (dd, J = 9.8, 6.6 Hz, 4H), 9.20 (d, J = 6.1 Hz, 1H), 9.11 (d, J = 7.2 Hz, 1H), 8.75 (d, J = 7.4 Hz, 1H), 8.16 (t, J = 16.8, 5.8 Hz, 6H), 7.97 (t, J = 7.6 Hz, 1H), 7.58 (d, J = 7.9 Hz, 1H), 4.82 (m, 2H), 4.53 (t, J = 5.5 Hz, 1H), 4.37 (m, 2H), 4.07 (t, J = 5.0 Hz, 2H), 3.76 (t, J = 5.0 Hz, 2H), 3.59(m, 2H), 3.49 (dd, J = 5.6, 4.1 Hz, 2H), 3.42 (m, 2H), 3.38 (s, 2H). ^{13}C NMR (101 MHz, DMSO-d_6): δ = 174.96, 169.25, 167.95, 156.11, 153.38, 153.28, 153.20, 153.14, 140.93, 138.91, 138.61, 138.56, 138.51, 138.48, 136.87, 131.01, 129.61, 129.56, 129.46, 125.57, 122.66, 120.05, 115.45, 114.15, 72.79, 70.99, 70.57, 70.40, 70.22, 69.38, 69.16, 60.65, 34.17, 31.73, 29.42, 29.13, 24.98, 22.53, 14.39. HRMS (ESI): m/z calculated for $C_{40}H_{32}N_8O_5Zn$ $[M + H]^+$, 769.1867; found, 769.1855. The purity was examined using HPLC (R_t = 6.52 min) and found to be >95%.

*2-(4-(6-((5-((2-Chloro-6-methylphenyl)carbamoyl)thiazol-2-yl)-amino)-2-methylpyrimidin-4-yl)piperazin-1-yl)ethyl (2-(2-(2-(2-(zinc(II)phthalocyanine-1-yloxy)ethoxy)ethoxy)ethoxy)ethyl) Succinate (**4**).* Compound **1** (0.64 g, 1.00 mmol) and EDCI (0.21 g, 1.09 mmol) were dissolved in 10 mL of DMF and stirred for 10 min; DMAP (0.052 g, 0.16 mmol) and compound **3** (1.00 g, 1.30 mmol) were then added, and the reaction was carried out for 24 h at rt. The mixture was evaporated under vacuum and purified using column chromatography (CH_2Cl_2/CH_3OH 20:1 v/v) to obtain a blue-green solid compound **4** (0.01 g, 7%). ^{1}H NMR (400 MHz, DMSO-d_6): δ = 11.47 (s, 1H), 9.91 (s, 1H), 9.25−8.92 (m, 6H), 8.61 (d, J = 7.4 Hz, 1H), 8.25 (s, 1H), 8.18−8.05 (m, 6H), 7.87 (t, J = 7.6 Hz, 1H), 7.44 (dd, J = 23.6, 4.9 Hz, 2H), 7.29 (dd, J = 7.7, 4.7 Hz, 2H), 6.00 (s, 1H), 4.79−4.71 (m, 2H), 4.38−4.30 (m, 2H), 4.05 (dd, J = 10.6, 6.1 Hz, 6H), 3.74 (dd, J = 5.8, 3.9 Hz, 2H), 3.68−3.46 (m, 8H), 3.41 (d, J = 19.6 Hz, 4H), 2.48 (s, 4H), 2.41 (d, J = 7.5 Hz, 4H), 2.39 (s, 3H), 2.26 (s, 3H). ^{13}C NMR (101 MHz, DMSO-d_6 with a trace amount of pyridine-d_5): δ = 174.41, 171.73, 171.61, 165.03, 162.49, 162.21, 159.87, 156.84, 155.75, 154.09, 153.12, 153.09, 153.02, 153.00, 152.93, 152.89, 152.87, 146.71, 140.80, 140.59, 138.75, 138.49, 138.17, 138.12, 138.07, 138.04, 133.50, 132.39, 130.64, 128.91, 128.04, 126.90, 125.63, 125.24, 122.20, 115.07, 113.81, 106.42, 82.53, 70.44, 70.03, 69.85, 69.74, 69.68, 68.95, 68.07, 63.31, 61.36, 52.18, 43.41, 38.45, 33.62, 31.17, 28.88, 28.78, 28.63, 28.58, 28.45, 28.39, 25.46, 24.42, 21.97, 18.23,13.83. HRMS (ESI): m/z calculated for $C_{66}H_{60}N_{15}O_9SZnCl$ $[M + H]^+$, 1338.3472; found, 1338.3441. The purity was examined using HPLC (R_t = 9.15 min) and found to be >95%.

Compound **5** was prepared according to the literature procedure.[67] The purity was examined using HPLC (R_t = 11.04 min) and found to be >95%.

Photophysical and Photochemical Characterization. The UV/vis spectra of **4** and **5** with different concentration gradients in DMF were measured in the range of 300−800 nm. To prevent aggregation and retain the stability of phthalocyanines, compounds **4** and **5** were dissolved in the mixed organic solvents of 78% DMAC (*N*,*N*-dimethylacetamide), 20% 1,2-propylene glycol, and 2% Cremophor EL (CEL) to form 1 mM stock solutions and then diluted with the same organic solvents to various concentrations. Meanwhile, the UV/vis spectra of **4** and **5** (both at 2.5 μM) in PBS or RPMI-1640 medium (containing 0.78% DMAC, 0.2% 1,2-propylene glycol, and 0.02% CEL) were also measured in the range of 300−800 nm. The fluorescence quantum yields (Φ_F) of both compounds were determined according to the formula

$$\Phi_F = \Phi_F^{std} \frac{FA_{std}}{F_{std}A}$$

where F, A, and η are the maximum emission peak integral area, the absorbance at a specific wavelength (610 nm), and the refractive index of the selected solvent, respectively. Unsubstituted zinc(II)

https://dx.doi.org/10.1021/acs.jmedchem.0c01072
J. Med. Chem. XXXX, XXX, XXX−XXX

phthalocyanine (ZnPc) was selected as the standard ($\Phi_{std\ F}$ = 0.28 in DMF).

The singlet oxygen quantum yield (Φ_Δ) was obtained using 1,3-diphenylisobenzofuran (DPBF) as a scavenger. Light (670 nm, 100 mW·cm^{-2}) was employed, and the absorbance of DPBF at 415 nm was measured every 10 s. The singlet oxygen quantum yields (Φ_Δ) of the two compounds were determined according to the formula

$$\Phi_\Delta = \Phi_\Delta^{std} \frac{kI_{abs}^{std}}{k^{std}I_{abs}}$$

where K and I are the DPBF degradation rate constant and the light absorption rate, respectively. Unsubstituted zinc(II) phthalocyanine was used as the standard (Φ_Δ = 0.56 in DMF).

HPLC Analysis. Analytical HPLC experiments were performed using an E2695 (Waters) binary HPLC pump with a Waters 2998 photodiode array detector. The solvents used for HPLC analysis were of HPLC grade. The conditions of HPLC were set as follows: solvent A = tetrahydrofuran (THF), solvent B = deionized water, and elution mode = isocratic: [50% A] and [50% B]. The total elution time was 30 min. The flow rate was fixed at 1.0 mL·min^{-1}.

Cellular Uptake. Approximately 2 × 10^5 CEM cells were inoculated in cell culture dishes for 24 h at 37 °C under 5% CO_2. Compounds **4** and **5** were dissolved in the mixed organic solvents of 78% DMAC, 20% 1,2-propylene glycol, and 2% CEL to form 1 mM stock solutions. Then, these stock solutions were diluted with the same organic solvents to 100 μM and further diluted with RPMI-1640 medium (HyClone) to 1 μM (containing 0.78% DMAC, 0.2% 1,2-propylene glycol, and 0.02% CEL). The medium was then exchanged with a fresh medium containing **4** and **5** (both at 1 μM). After 1 h of incubation, the medium was centrifuged to remove drugs that were not ingested, and then CEM cells were collected. For the dasatinib inhibition assay, the CEM cells were pretreated with or without dasatinib (10 μM) for 1 h, followed by incubation with **4** (1 μM) for a further 1 h. After 1 h of incubation, the medium was centrifuged to remove drugs that were not ingested, and then the CEM cells were collected. For the selectivity assay of **4**, the HELF and CEM cells were inoculated in the same cell culture dish, which contains approximately 1 × 10^5 cells of each kind, and incubated for 24 h at 37 °C under 5% CO_2. All cell culture dishes were randomly divided into two groups, **4** and **5** (both at 1 μM). After 1 h of incubation, the medium was centrifuged to remove drugs that were not ingested, and then CEM cells were collected. At the same time, HELF cells were washed, digested, and collected. The fluorescence intensities of all groups were detected by cell flow cytometry. All control groups were treated with a fresh medium (containing 0.78% DMAC, 0.2% 1,2-propylene glycol, and 0.02% CEL).

***In Vitro* Photodynamic Cytostatic Activities.** Approximately 1 × 10^4 CEM cells in RPMI-1640 medium and HELF cells in Dulbecco's modified Eagle's medium (DMEM) were seeded per well in different 96-well cell plates and incubated for 24 h at 37 °C under 5% CO_2. All compounds were prepared as mentioned above to form 1 μM solutions (containing 0.78% DMAC, 0.2% 1,2-propylene glycol, and 0.02% CEL) and then diluted with RPMI-1640 medium to various concentrations. The control group was treated with a fresh medium (containing 0.78% DMAC, 0.2% 1,2-propylene glycol, and 0.02% CEL). The compounds were diluted to the required concentration and added to the corresponding wells. After 1 h of incubation, for the CEM cells, the medium was centrifuged at 1000 rpm for 4 min to remove the supernatant, and then the cells were resuspended and transferred to a new 96-well plate. The HELF cells were washed three times with PBS and transferred to the new DMEM medium. All plates for photocytotoxicity were irradiated with a LED light source (λ = 670 nm, 4 mW·cm^{-2}, 0.48 J·cm^{-2}) for 2 min and incubated for 24 h. Then, 20 μL of CCK-8 solution (Dojindo. Japan) was added to each well and incubated for 4 h. The absorbance at 450 nm was detected on the microplate reader. The steps of the dark cytotoxic experiments were consistent with those of the photocytotoxicity experiments but without irradiation. The data and the concentration IC_{50} were analyzed and calculated using the GraphPad Prism 6.0 software.

Subcellular Localization. Approximately 1 × 10^4 CEM cells were seeded in a cell culture dish containing 1 μM **4** and **5** (containing 0.78% DMAC, 0.2% 1,2-propylene glycol, and 0.02% CEL). After 24 h of incubation, the mixture was centrifuged at 1000 rpm for 4 min to remove the supernatant. After centrifugation, the cells were resuspended in a fresh medium and stained with Mito-Tracker Green FM (Beijing Dingguo Biotechnology Co., Ltd., 2 μM in a culture medium stained for 20 min), Lyso-Tracker DND-26 (Beijing Dingguo Biotechnology Co., Ltd., 2 μM in a culture medium stained for 25 min), and Hoechst 33258 (Beijing Dingguo Biotechnology Co., Ltd., 1 μM in a culture medium stained for 30 min), respectively. Then, the cells were centrifuged to remove the supernatant. Finally, the cells were resuspended by a small amount of PBS and then placed in a cell culture dish prior to photographing. The cells were then viewed with an Olympus FV1000 laser confocal microscope equipped with a 405 nm or 488 nm multiargon laser and a 633 nm diode laser. All of the trackers were excited at 405 nm and monitored at 425−475 nm (Hoechst 33258) or excited at 488 nm and monitored at 510−570 nm (Mito-Tracker Green FM, Lyso-Tracker DND-26), while **4** and **5** were both excited at 633 nm and monitored at 650−750 nm. The images were digitized and analyzed using the FV10-ASW software.

***In Vivo* Tumor Tissue Targeting.** The experiment used female nude mice of 4−5 weeks (17−20 g, purchased from Shanghai SLAC Laboratory Animal Co., Ltd, China). All mice were maintained and handled in accordance with the recommendations of the Animal Care and Use Committee (IACUC). All mice were randomly divided into two groups (n = 3), and all laboratory supplies and procedures were sterile. Briefly, 200 μL of CEM cells (1 x 10^{7}cells) were subcutaneously inoculated into the right forelimbs of mice for 14 days. Compounds **4** and **5** were dissolved in 78% DMAC, 20% 1,2-propylene glycol, and 2% CEL to obtain 2.5 mM stock solutions. Then, these stock solutions were diluted with PBS to 25 μM (containing 0.78% DMAC, 0.2% 1,2-propylene glycol, and 0.02% CEL). Once the tumor grew to 50−100 mm^3, 200 μL of **4** and **5** (0.25 μmol·kg^{-1}) were injected into the mice by tail vein injection. All mice were observed using a fluorescence molecular tomography FMT 2500FM. LX. instrument. The accumulation of drugs in tumors at different time points (0, 2, 6, 12, 24 h) was detected by three-dimensional fluorescence imaging. The images and the average drug concentrations were obtained using software TrueQuant version 3.0 (PerkinElmer).

***In Vivo* Photodynamic Activities.** All mice with tumor were randomly divided into four groups (n = 5): (a) **4**, (b) **5**, (c) dasatinib, and (d) control. All compounds were dissolved in 78% DMAC, 20% 1,2-propylene glycol, and 2% CEL, respectively, to obtain 7.5 mM stock solutions and diluted with PBS to 75 μM (containing 0.78% DMAC, 0.2% 1,2-propylene glycol, and 0.02% CEL). Then, 200 μL of **4**, **5**, and dasatinib (0.75 μmol·kg^{-1}) were injected into the mice by tail vein injection. The control group was treated with 200 μL of PBS (containing 0.78% DMAC, 0.2% 1,2-propylene glycol, and 0.02% CEL). The tumor site of the mice was irradiated by a laser (λ = 670 nm, 50 mW·cm^{-2}, 10 min) at 6 h post injection. After treatment, the weight of the mice was measured. The length (a) and width (b) of the tumor were measured using vernier caliper every other day. The tumor volume was calculated using the formula $ab^2/2$. At 16 days post treatment, all mice were sacrificed, and major organs and tumors were removed and weighed.

Histological Analysis. All representative tumors and major organs in each group were collected at 16 days after treatment and fixed in 10% formalin. The paraffin sections were stained with hematoxylin and eosin (H&E).

Immunity Response Study. The tissue sections of the four groups (n = 3) were first dehydrated and then rehydrated, immersed in an antigen repair working solution, and repaired by microwave. Then, the tissue sections were incubated with the primary antibody at room temperature for the corresponding durations. After incubation, the goat antirabbit or goat antimouse rabbit antibody diluted in

https://dx.doi.org/10.1021/acs.jmedchem.0c01072
J. Med. Chem. XXXX, XXX, XXX−XXX

proportion was used for secondary incubation. Multiplex immunofluorescence staining was obtained by PPD650 fluorescence staining, and antigen retrieval was performed again. Sequentially, the different primary antibodies were applied, the secondary antibody which horseradish peroxidase-conjugated were incubated and tyramide signal amplification. Finally, the remaining washing solution in the sections was removed, and the nuclei were incubated with 4′-6′-diamidino-2-phenylindole (DAPI) at room temperature for 10 min. The sections were dipped in TBST buffer for 3 min at room temperature and washed for 2 min with sterile water. A strong antiquenching sealer and nail polish were added when the sections were slightly dry. The stained tissue slides were observed under a fluorescence microscope.

■ ASSOCIATED CONTENT

Supporting Information

The Supporting Information is available free of charge at https://pubs.acs.org/doi/10.1021/acs.jmedchem.0c01072.

Electronic absorption spectra of **4** and **5** in PBS or RPMI-1640 medium; fluorescence spectra of **4** and **5** in DMF; absorbance spectra of DPBF at 415 nm; cytotoxicity of dasatinib toward CEM cells at high concentrations; cytotoxicity of compounds toward HELF cells with/without light illumination; subcellular localization of **5**; H&E staining of different organs in the four groups; staining of different antibodies in **5**, dasatinib, and control groups; and ^{1}H NMR, ^{13}C NMR, and HRMS of all new compounds and HPLC of compounds **3**, **4**, and **5** (PDF)

Molecular formula strings (CSV)

■ AUTHOR INFORMATION

Corresponding Authors

Juanjuan Chen − *National & Local Joint Biomedical Engineering Research Center on Photodynamic Technologies, State Key Laboratory of Photocatalysis on Energy and Environment, College of Chemistry, Fuzhou University, Fuzhou 350116, Fujian, P. R. China;* orcid.org/0000-0002-9148-2206; Email: chenjuanjuan@fzu.edu.cn

Jinping Xue − *National & Local Joint Biomedical Engineering Research Center on Photodynamic Technologies, State Key Laboratory of Photocatalysis on Energy and Environment, College of Chemistry, Fuzhou University, Fuzhou 350116, Fujian, P. R. China;* orcid.org/0000-0001-6952-0475; Email: xuejinping66@fzu.edu.cn

Authors

Gankun Yuan − *National & Local Joint Biomedical Engineering Research Center on Photodynamic Technologies, State Key Laboratory of Photocatalysis on Energy and Environment, College of Chemistry, Fuzhou University, Fuzhou 350116, Fujian, P. R. China*

Mengyu Yao − *National & Local Joint Biomedical Engineering Research Center on Photodynamic Technologies, State Key Laboratory of Photocatalysis on Energy and Environment, College of Chemistry, Fuzhou University, Fuzhou 350116, Fujian, P. R. China*

Huihui Lv − *National & Local Joint Biomedical Engineering Research Center on Photodynamic Technologies, State Key Laboratory of Photocatalysis on Energy and Environment, College of Chemistry, Fuzhou University, Fuzhou 350116, Fujian, P. R. China*

Xiao Jia − *National & Local Joint Biomedical Engineering Research Center on Photodynamic Technologies, State Key Laboratory of Photocatalysis on Energy and Environment, College of Chemistry, Fuzhou University, Fuzhou 350116, Fujian, P. R. China*

Complete contact information is available at: https://pubs.acs.org/10.1021/acs.jmedchem.0c01072

Author Contributions

The manuscript was written through the contributions of all authors. All authors have given approval to the final version of the manuscript.

Funding

The National Natural Science Foundation of China (Project No. 81703345) and the National Health and Family Planning Commission jointly established a scientific research fund (Project No. WKJ2016-2-14).

Notes

The authors declare no competing financial interest.

■ ACKNOWLEDGMENTS

We thank WuXi AppTec Co., Ltd (WuXi, China) for mice care and operation during *in vivo* experiments. We thank Panovue Biotechnology (Beijing) Co. Ltd for technical support with immunofluorescent staining.

■ ABBREVIATIONS USED

PDT, photodynamic therapy; LCK, lymphocyte-specific protein tyrosine kinase; ALL, acute lymphoblastic leukemia; T-ALL, T-cell acute lymphoblastic leukemia; ROS, reactive oxygen species; PS, photosensitizer; DCs, dendritic cells; DBU, diazabicyclo[5.4.0]undec-7-ene; DMAP, 4-dimethylaminopyridine; EDCI, 1-(3-dimethylaminopropyl)-3-ethylcarbodiimide hydrochloride; DMF, *N*,*N*-dimethylformamide; ZnPc, zinc phthalocyanine; HPLC, high-performance liquid chromatography; Φ_F, fluorescence quantum yield; Φ_Δ, singlet oxygen quantum yield; DPBF, 1,3-diphenylisobenzofuran; SEM, standard error of the mean; CCK-8, cell counting kit-8; IC_{50}, dye concentration required to kill 50% of the cells; DMAC, *N*,*N*-dimethylacetamide; FMT, fluorescence molecular tomography; PBS, phosphate-buffered saline; NK, natural killer; DAPI, 4′,6-diamidino-2-phenylindole; RPMI-1640, Roswell Park Memorial Institute 1640; DMEM, Dulbecco's modified Eagle's medium; THF, tetrahydrofuran; CEL, Cremophor EL

■ REFERENCES

(1) Paul, S.; Kantarjian, H.; Jabbour, E. J. Adult acute lymphoblastic leukemia. *Mayo Clin. Proc.* **2016**, *91*, 1645−1666.

(2) Styczynski, J. A step forward in acute lymphoblastic leukemia. *Transl. Pediatr.* **2012**, *1*, 68−69.

(3) Terwilliger, T.; Abdul-Hay, M. Acute lymphoblastic leukemia: a comprehensive review and 2017 update. *Blood Cancer J.* **2017**, *7*, No. e577.

(4) Fang, Z.; Wang, X.; Sun, Y.; Fan, R.; Liu, Z.; Guo, R.; Xie, D. Sgc8 aptamer targeted glutathione-responsive nanoassemblies containing Ara-C prodrug for the treatment of acute lymphoblastic leukemia. *Nanoscale* **2019**, *11*, 23000−23012.

(5) Miller, K. D.; Nogueira, L.; Mariotto, A. B.; Rowland, J. H.; Yabroff, K. R.; Alfano, C. M.; Jemal, A.; Kramer, J. L.; Siegel, R. L. Cancer treatment and survivorship statistics, 2019. *Ca-Cancer J. Clin.* **2019**, *69*, 363−385.

(6) Portell, C.; Advani, A. Antibody therapy for acute lymphoblastic leukemia. *Curr. Hematol. Malig. Rep.* **2012**, *7*, 153−159.

(7) Bassan, R.; Hoelzer, D. Modern therapy of acute lymphoblastic leukemia. *J. Clin. Oncol.* **2011**, *29*, 532−543.

(8) Sas, V.; Moisoiu, V.; Teodorescu, P.; Tranca, S.; Pop, L.; Iluta, S.; Pasca, S.; Blag, C.; Man, S.; Roman, A.; Constantinescu, C.; Rus, I.; Buse, M.; Fetica, B.; Marian, M.; Selicean, C.; Berindan-Neagoe, I.; Petrushev, B.; Bumbea, H.; Tanase, A.; Zdrenghea, M.; Fuji, S.; Kitano, S.; Tomuleasa, C.; Romanian Soc Bone Marrow, T. Approach to the adult acute lymphoblastic leukemia patient. *J. Clin. Med.* **2019**, *8*, 1175.
(9) Aldoss, I.; Stein, A. S. Advances in adult acute lymphoblastic leukemia therapy. *Leuk. Lymphoma* **2018**, *59*, 1033−1050.
(10) Araujo, J.; Logothetis, C. Dasatinib: a potent SRC inhibitor in clinical development for the treatment of solid tumors. *Cancer Treat. Rev.* **2010**, *36*, 492−500.
(11) Malkan, U. Y.; Gunes, G.; Etgul, S.; Aslan, T.; Aydin, S.; Haznedaroglu, I. C. Reply: management of De Novo CML and imatinib-induced acute rhabdomyolysis with the second-generation TKI, dasatinib. *Ann. Pharmacother.* **2016**, *50*, 336.
(12) Kostos, L.; Burbury, K.; Srivastava, G.; Prince, H. M. Gastrointestinal bleeding in a chronic myeloid leukaemia patient precipitated by dasatinib-induced platelet dysfunction: case report. *Platelets* **2015**, *26*, 809−811.
(13) Aleshin, A.; Finn, R. S. SRC: a century of science brought to the clinic. *Neoplasia* **2010**, *12*, 599−607.
(14) Lee, P. C.; Lee, H. J.; Kakadiya, R.; Sanjiv, K.; Su, T. L.; Lee, T. C. Multidrug-resistant cells overexpressing P-glycoprotein are susceptible to DNA crosslinking agents due to attenuated Src/nuclear EGFR cascade-activated DNA repair activity. *Oncogene* **2013**, *32*, 1144−1154.
(15) Yeatman, T. J. A renaissance for SRC. *Nat. Rev. Cancer* **2004**, *4*, 470−480.
(16) Serafin, V.; Capuzzo, G.; Milani, G.; Minuzzo, S. A.; Pinazza, M.; Bortolozzi, R.; Bresolin, S.; Porcu, E.; Frasson, C.; Indraccolo, S.; Basso, G.; Accordi, B. Glucocorticoid resistance is reverted by LCK inhibition in pediatric T-cell acute lymphoblastic leukemia. *Blood* **2017**, *130*, 2750−2761.
(17) Joosten, M.; Seitz, V.; Zimmermann, K.; Sommerfeld, A.; Berg, E.; Lenze, D.; Leser, U.; Stein, H.; Hummel, M. Histone acetylation and DNA demethylation of T cells result in an anaplastic large cell lymphoma-like phenotype. *Haematologica* **2013**, *98*, 247−254.
(18) Laukkanen, S.; Gronroos, T.; Polonen, P.; Kuusanmaki, H.; Mehtonen, J.; Cloos, J.; Ossenkoppele, G.; Gjertsen, B.; Oystein, B.; Heckman, C.; Heinaniemi, M.; Kontro, M.; Lohi, O. In silico and preclinical drug screening identifies dasatinib as a targeted therapy for T-ALL. *Blood Cancer J.* **2017**, *7*, No. e604.
(19) Sun, Y.; Sun, Z.-l. Transferrin-conjugated polymeric nanomedicine to enhance the anticancer efficacy of edelfosine in acute myeloid leukemia. *Biomed. Pharmacother.* **2016**, *83*, 51−57.
(20) Hareedy, M. S.; El Desoky, E. S.; Woillard, J.-B.; Thabet, R. H.; Ali, A. M.; Marquet, P.; Picard, N. Genetic variants in 6-mercaptopurine pathway as potential factors of hematological toxicity in acute lymphoblastic leukemia patients. *Pharmacogenomics* **2015**, *16*, 1119−1133.
(21) Qiu, J.; Cheng, R.; Zhang, J.; Sun, H.; Deng, C.; Meng, F.; Zhong, Z. Glutathione-sensitive hyaluronic acid-mercaptopurine prodrug linked via carbonyl vinyl sulfide: a robust and CD44-targeted nanomedicine for leukemia. *Biomacromolecules* **2017**, *18*, 3207−3214.
(22) Celli, J. P.; Spring, B. Q.; Rizvi, I.; Evans, C. L.; Samkoe, K. S.; Verma, S.; Pogue, B. W.; Hasan, T. Imaging and photodynamic therapy: mechanisms, monitoring, and optimization. *Chem. Rev.* **2010**, *110*, 2795−2838.
(23) Lovell, J. F.; Liu, T. W. B.; Chen, J.; Zheng, G. Activatable photosensitizers for imaging and therapy. *Chem. Rev.* **2010**, *110*, 2839−2857.
(24) Li, F.; Chen, C.; Yang, X.; He, X.; Zhao, Z.; Li, J.; Yu, Y.; Yang, X.; Wang, J. Acetal-linked hyperbranched polyphosphoester nanocarriers loaded with chlorin e6 for pH-activatable photodynamic therapy. *ACS Appl. Mater. Interfaces* **2018**, *10*, 21198−21205.
(25) Zhou, Z.; Song, J.; Nie, L.; Chen, X. Reactive oxygen species generating systems meeting challenges of photodynamic cancer therapy. *Chem. Soc. Rev.* **2016**, *45*, 6597−6626.
(26) Guo, R.; Yang, G.; Feng, Z.; Zhu, Y.; Yang, P.; Song, H.; Wang, W.; Huang, P.; Zhang, J. Glutathione-induced amino-activatable micellar photosensitization platform for synergistic redox modulation and photodynamic therapy. *Biomater. Sci.* **2018**, *6*, 1238−1249.
(27) Zhang, L.; Ji, Z.; Zhang, J.; Yang, S. Photodynamic therapy enhances skin cancer chemotherapy effects through autophagy regulation. *Photodiagn. Photodyn. Ther.* **2019**, *28*, 159−165.
(28) Abdel-Hady, E. S.; Martin-Hirsch, P.; Duggan-Keen, M.; Stern, P. L.; Moore, J. V.; Corbitt, G.; Kitchener, H. C.; Hampson, I. N. Immunological and viral factors associated with the response of vulval intraepithelial neoplasia to photodynamic therapy. *Cancer Res.* **2001**, *61*, 192−196.
(29) Agostinis, P.; Berg, K.; Cengel, K. A.; Foster, T. H.; Girotti, A. W.; Gollnick, S. O.; Hahn, S. M.; Hamblin, M. R.; Juzeniene, A.; Kessel, D.; Korbelik, M.; Moan, J.; Mroz, P.; Nowis, D.; Piette, J.; Wilson, B. C.; Golab, J. Photodynamic therapy of cancer: an update. *Ca-Cancer J. Clin.* **2011**, *61*, 250−281.
(30) Brackett, C. M.; Gollnick, S. O. Photodynamic therapy enhancement of anti-tumor immunity. *Photochem. Photobiol. Sci.* **2011**, *10*, 649−652.
(31) Sandra, O. G.; Barbara, O.; Patricia, M. Induction of anti-tumor immunity by photodynamic therapy (PDT). *Proc. SPIE* **2006**, *6087*, No. 60870E.
(32) Mroz, P.; Hashmi, J. T.; Huang, Y.-Y.; Lange, N.; Hamblin, M. R. Stimulation of anti-tumor immunity by photodynamic therapy. *Expert Rev. Clin. Immunol.* **2011**, *7*, 75−91.
(33) He, C.; Duan, X.; Guo, N.; Chan, C.; Poon, C.; Weichselbaum, R. R.; Lin, W. Core-shell nanoscale coordination polymers combine chemotherapy and photodynamic therapy to potentiate checkpoint blockade cancer immunotherapy. *Nat. Commun.* **2016**, *7*, No. 12499.
(34) Lu, K.; He, C.; Guo, N.; Chan, C.; Ni, K.; Weichselbaum, R. R.; Lin, W. Chlorin-based nanoscalemetal−organic framework systemically rejects colorectal cancers via synergistic photodynamic therapy and checkpoint blockade immunotherapy. *J. Am. Chem. Soc.* **2016**, *138*, 12502−12510.
(35) Krosl, G.; Korbelik, M.; Dougherty, G.; Krosl, G.; Korbelik, M.; Dougherty, G. J. Induction of cell infiltration into murine SCCVII tumor by photofrin-based photodynamic therapy. *Br. J. Cancer* **1995**, *71*, 549−555.
(36) Donohoe, C.; Senge, M. O.; Arnaut, L. G.; Gomes-da-Silva, L. C. Cell death in photodynamic therapy: From oxidative stress to anti-tumor immunity. *Biochim. Biophys. Acta, Rev. Cancer* **2019**, *1872*, No. 188308.
(37) Hwang, H. S.; Shin, H.; Han, J.; Na, K. Combination of photodynamic therapy (PDT) and anti-tumor immunity in cancer therapy. *J. Pharm. Investig.* **2018**, *48*, 143−151.
(38) Castano, A. P.; Mroz, P.; Hamblin, M. R. Photodynamic therapy and anti-tumour immunity. *Nat. Rev. Cancer* **2006**, *6*, 535−545.
(39) Chi, J.; Ma, Q.; Shen, Z.; Ma, C.; Zhu, W.; Han, S.; Liang, Y.; Cao, J.; Sun, Y. Targeted nanocarriers based on iodinated-cyanine dyes as immunomodulators for synergistic phototherapy. *Nanoscale* **2020**, *12*, 11008−11025.
(40) Feng, C.; Zhu, D.; Chen, L.; Lu, Y.; Liu, J.; Kim, N. Y.; Liang, S.; Zhang, X.; Lin, Y.; Ma, Y.; Dong, C. Targeted delivery of chlorin e6 via redox sensitive diselenide-containing micelles for improved photodynamic therapy in cluster of differentiation 44-overexpressing breast cancer. *Front. Pharmacol.* **2019**, *10*, 369.
(41) Yan, S.; Huang, Q.; Chen, J.; Song, X.; Chen, Z.; Huang, M.; Xu, P.; Zhang, J. Tumor-targeting photodynamic therapy based on folate-modified polydopamine nanoparticles. *Int. J. Nanomed.* **2019**, *14*, 6799−6812.
(42) Huang, Z.; Xu, H.; Meyers, A. D.; Musani, A. I.; Wang, L.; Tagg, R.; Barqawi, A. B.; Chen, Y. K. Photodynamic therapy for treatment of solid tumors-potential and technical challenges. *Technol. Cancer Res. Treat.* **2008**, *7*, 309−320.
(43) Sharman, W. M.; Allen, C. M.; van Lier, J. E. Photodynamic therapeutics: basic principles and clinical applications. *Drug Discovery Today* **1999**, *4*, 507−517.

https://dx.doi.org/10.1021/acs.jmedchem.0c01072
J. Med. Chem. XXXX, XXX, XXX−XXX

(44) Chen, D.; Tang, Y.; Zhu, J.; Zhang, J.; Song, X.; Wang, W.; Shao, J.; Huang, W.; Chen, P.; Dong, X. Photothermal-pH-hypoxia responsive multifunctional nanoplatform for cancer photo-chemo therapy with negligible skin phototoxicity. *Biomaterials* **2019**, *221*, No. 119422.
(45) Chen, J.; Li, D.; Huo, B.; Zhang, F.; Zhao, X.; Yuan, G.; Chen, D.; Song, M.; Xue, J. Epidermal growth factor receptor-targeted delivery of a singlet-oxygen sensitizer with thermal controlled release for efficient anticancer therapy. *Mol. Pharmaceutics* **2019**, *16*, 3703−3710.
(46) Sebak, A. A.; Gomaa, I. E. O.; ElMeshad, A. N.; AbdelKader, M. H. Targeted photodynamic-induced singlet oxygen production by peptide-conjugated biodegradable nanoparticles for treatment of skin melanoma. *Photodiagn. Photodyn. Ther.* **2018**, *23*, 181−189.
(47) Lütje, S.; Heskamp, S.; Franssen, G. M.; Frielink, C.; Kip, A.; Hekman, M.; Fracasso, G.; Colombatti, M.; Herrmann, K.; Boerman, O. C.; Gotthardt, M.; Rijpkema, M. Development and characterization of a theranostic multimodal anti-PSMA targeting agent for imaging, surgical guidance, and targeted photodynamic therapy of PSMA-expressing tumors. *Theranostics* **2019**, *9*, 2924−2938.
(48) Fernandes, S. R. G.; Fernandes, R.; Sarmento, B.; Pereira, P. M. R.; Tomé, J. P. C. Photoimmunoconjugates: novel synthetic strategies to target and treat cancer by photodynamic therapy. *Org. Biomol. Chem.* **2019**, *17*, 2579−2593.
(49) Bao, R.; Wang, Y.; Lai, J.; Zhu, H.; Zhao, Y.; Li, S.; Li, N.; Huang, J.; Yang, Z.; Wang, F.; Liu, Z. Enhancing anti-PD-1/PD-L1 immune checkpoint inhibitory cancer therapy by CD276-targeted photodynamic ablation of tumor cells and tumor vasculature. *Mol. Pharmaceutics* **2019**, *16*, 339−348.
(50) Xu, W.; Qian, J.; Hou, G.; Wang, Y.; Wang, J.; Sun, T.; Ji, L.; Suo, A.; Yao, Y. A dual-targeted hyaluronic acid-gold nanorod platform with triple-stimuli responsiveness for photodynamic/photothermal therapy of breast cancer. *Acta Biomater.* **2019**, *83*, 400−413.
(51) Mao, C.; Qu, P.; Miley, M. J.; Zhao, Y.; Li, Z.; Ming, X. P-glycoprotein targeted photodynamic therapy of chemoresistant tumors using recombinant Fab fragment conjugates. *Biomater. Sci.* **2018**, *6*, 3063−3074.
(52) Feng, Y.; Chen, H.; Wu, Y.; Que, I.; Tamburini, F.; Baldazzi, F.; Chang, Y.; Zhang, H. Optical imaging and pH-awakening therapy of deep tissue cancer based on specific upconversion nanophotosensitizers. *Biomaterials* **2020**, *230*, No. 119637.
(53) Dai, J.; Li, Y.; Long, Z.; Jiang, R.; Zhuang, Z.; Wang, Z.; Zhao, Z.; Lou, X.; Xia, F.; Tang, B. Z. Efficient near-infrared photosensitizer with aggregation-induced emission for imaging-guided photodynamic therapy in multiple xenograft tumor models. *ACS Nano* **2020**, *14*, 854−866.
(54) Haimov-Talmoud, E.; Harel, Y.; Schori, H.; Motiei, M.; Atkins, A.; Popovtzer, R.; Lellouche, J.-P.; Shefi, O. Magnetic targeting of mTHPC to improve the selectivity and efficiency of photodynamic therapy. *ACS Appl. Mater. Interfaces* **2019**, *11*, 45368−45380.
(55) Yang, G.; Chen, C.; Zhu, Y.; Liu, Z.; Xue, Y.; Zhong, S.; Wang, C.; Gao, Y.; Zhang, W. GSH-activatable NIR nanoplatform with mitochondria targeting for enhancing tumor-specific therapy. *ACS Appl. Mater. Interfaces* **2019**, *11*, 44961−44969.
(56) Liu, W.; Zhang, K.; Zhuang, L.; Liu, J.; Zeng, W.; Shi, J.; Zhang, Z. Aptamer/photosensitizer hybridized mesoporous MnO_2 based tumor cell activated ROS regulator for precise photodynamic therapy of breast cancer. *Colloid Surf., B* **2019**, *184*, No. 110536.
(57) Zhang, Y.; Sun, T.; Jiang, C. Biomacromolecules as carriers in drug delivery and tissue engineering. *Acta Pharm. Sin. B* **2018**, *8*, 34−50.
(58) Lin, W.; Huang, Y.-w.; Zhou, X.-D.; Ma, Y. In vitro toxicity of silica nanoparticles in human lung cancer cells. *Toxicol. Appl. Pharmacol.* **2006**, *217*, 252−259.
(59) Soenen, S. J.; Rivera-Gil, P.; Montenegro, J.-M.; Parak, W. J.; De Smedt, S. C.; Braeckmans, K. Cellular toxicity of inorganic nanoparticles: common aspects and guidelines for improved nanotoxicity evaluation. *Nano Today* **2011**, *6*, 446−465.
(60) Fadeel, B.; Garcia-Bennett, A. E. Better safe than sorry: understanding the toxicological properties of inorganic nanoparticles manufactured for biomedical applications. *Adv. Drug Delivery Rev.* **2010**, *62*, 362−374.
(61) Elsaesser, A.; Howard, C. V. Toxicology of nanoparticles. *Adv. Drug Delivery Rev.* **2012**, *64*, 129−137.
(62) Song, G.; Hao, J.; Liang, C.; Liu, T.; Gao, M.; Cheng, L.; Hu, J.; Liu, Z. Degradable molybdenum oxide nanosheets with rapid clearance and efficient tumor homing capabilities as a therapeutic nanoplatform. *Angew. Chem., Int. Ed.* **2016**, *55*, 2122−2126.
(63) Oka, T.; Matsuoka, K. I.; Utsunomiya, A. Sensitive photodynamic detection of adult T-cell leukemia/lymphoma and specific leukemic cell death induced by photodynamic therapy: current status in hematopoietic malignancies. *Cancers* **2020**, *12*, 335.
(64) Xu, L.; Zhang, X.; Cheng, W.; Wang, Y.; Yi, K.; Wang, Z.; Zhang, Y.; Shao, L.; Zhao, T. Hypericin-photodynamic therapy inhibits the growth of adult T-cell leukemia cells through induction of apoptosis and suppression of viral transcription. *Retrovirology* **2019**, *16*, 5.
(65) Aksakal, N. E.; Kazan, H. H.; Eçik, E. T.; Yuksel, F. A novel photosensitizer based on a ruthenium(ii) phenanthroline bis-(perylenediimide) dyad: synthesis, generation of singlet oxygen and in vitro photodynamic therapy. *New J. Chem.* **2018**, *42*, 17538−17545.
(66) Păunescu, E.; Clavel, C. M.; Nowak-Sliwinska, P.; Griffioen, A. W.; Dyson, P. J. Improved angiostatic activity of dasatinib by modulation with hydrophobic chains. *ACS Med. Chem. Lett.* **2015**, *6*, 313−317.
(67) Zhang, F.-L.; Huang, Q.; Zheng, K.; Li, J.; Liu, J.-Y.; Xue, J.-P. A novel strategy for targeting photodynamic therapy. Molecular combo of photodynamic agent zinc(ii) phthalocyanine and small molecule target-based anticancer drug erlotinib. *Chem. Commun.* **2013**, *49*, 9570−9572.
(68) Würthner, F.; Kaiser, T. E.; Saha-Moller, C. R. J-aggregates: from serendipitous discovery to supramolecular engineering of functional dye materials. *Angew. Chem., Int. Ed.* **2011**, *50*, 3376−3410.
(69) Walczak, P. B.; Eisfeld, A.; Briggs, J. S. Exchange narrowing of the J band of molecular dye aggregates. *J. Chem. Phys.* **2008**, *128*, No. 044505.
(70) Egorov, V. V. Theory of the J-band: from the Frenkel exciton to charge transfer. *Phys. Procedia* **2009**, *2*, 223−326.
(71) Scalise, I.; Durantini, E. N. Synthesis, properties, and photodynamic inactivation of Escherichia coli using a cationic and a noncharged Zn(II) pyridyloxyphthalocyanine derivatives. *Bioorg. Med. Chem.* **2005**, *13*, 3037−3045.
(72) Savić, R.; Eisenberg, A.; Maysinger, D. Block copolymer micelles as delivery vehicles of hydrophobic drugs: Micelle−cell interactions. *J. Drug Target.* **2006**, *14*, 343−355.
(73) Master, A. M.; Qi, Y.; Oleinick, N. L.; Gupta, A. S. EGFR-mediated intracellular delivery of Pc 4 nanoformulation for targeted photodynamic therapy of cancer: in vitro studies. *Nanomedicine* **2012**, *8*, 655−664.
(74) Shi, Y.; Beckett, M. C.; Blair, H. J.; Tirtakusuma, R.; Nakjang, S.; Enshaei, A.; Halsey, C.; Vormoor, J.; Heidenreich, O.; Krippner-Heidenreich, A.; van Delft, F. W. Phase II-like murine trial identifies synergy between dexamethasone and dasatinib in T-cell acute lymphoblastic leukemia. *Haematologica* **2020**, *105*, No. 241026.
(75) Harr, M. W.; Caimi, P. F.; McColl, K. S.; Zhong, F.; Patel, S. N.; Barr, P. M.; Distelhorst, C. W. Inhibition of Lck enhances glucocorticoid sensitivity and apoptosis in lymphoid cell lines and in chronic lymphocytic leukemia. *Cell Death Differ.* **2010**, *17*, 1381−1391.
(76) Ethirajan, M.; Chen, Y.; Joshi, P.; Pandey, R. K. The role of porphyrin chemistry in tumor imaging and photodynamic therapy. *Chem. Soc. Rev.* **2011**, *40*, 340−362.
(77) Pan, L. M.; Liu, J. A.; Shi, J. L. Intranuclear photosensitizer delivery and photosensitization for enhanced photodynamic therapy with ultralow irradiance. *Adv. Funct. Mater.* **2014**, *24*, 7318−7327.
(78) Yu, Z.; Sun, Q.; Pan, W.; Li, N.; Tang, B. A near-infrared triggered nanophotosensitizer inducing domino effect on mitochon-

https://dx.doi.org/10.1021/acs.jmedchem.0c01072
J. Med. Chem. XXXX, XXX, XXX−XXX

drial reactive oxygen species burst for cancer therapy. *ACS Nano* **2015**, *9*, 11064−11074.
(79) Rajaputra, P.; Nkepang, G.; Watley, R.; You, Y. Synthesis and in vitro biological evaluation of lipophilic cation conjugated photosensitizers for targeting mitochondria. *Bioorg. Med. Chem.* **2013**, *21*, 379−387.
(80) Han, K.; Zhang, W. Y.; Zhang, J.; Lei, Q.; Wang, S. B.; Liu, J. W.; Zhang, X. Z.; Han, H. Y. Acidity-triggered tumor-targeted chimeric peptide for enhanced intra-nuclear photodynamic therapy. *Adv. Funct. Mater.* **2016**, *26*, 4351−4361.
(81) Sivori, S.; Vacca, P.; Del Zotto, G.; Munari, E.; Mingari, M. C.; Moretta, L. Human NK cells: surface receptors, inhibitory checkpoints, and translational applications. *Cell Mol. Immunol.* **2019**, *16*, 430−441.
(82) Chiossone, L.; Dumas, P. Y.; Vienne, M.; Vivier, E. Natural killer cells and other innate lymphoid cells in cancer. *Nat. Rev. Immunol.* **2018**, *18*, 671−688.
(83) DeNardo, D. G.; Ruffell, B. Macrophages as regulators of tumour immunity and immunotherapy. *Nat. Rev. Immunol.* **2019**, *19*, 369−382.
(84) Gordon, S.; Pluddemann, A. Tissue macrophages: heterogeneity and functions. *BMC Biol.* **2017**, *15*, 53.
(85) Yunna, C.; Mengru, H.; Lei, W.; Weidong, C. Macrophage M1/M2 polarization. *Eur. J. Pharmacol.* **2020**, *877*, No. 173090.

https://dx.doi.org/10.1021/acs.jmedchem.0c01072
J. Med. Chem. XXXX, XXX, XXX−XXX